

CrossMark
click for updatesCite this: *J. Mater. Chem. A*, 2015, **3**,
2942

Structure and ionic conductivity of liquid crystals having propylene carbonate units†

Andreas Eisele,^a Konstantinos Kyriakos,^b Rajesh Bhandary,^{cd} Monika Schönhoff,^c Christine M. Papadakis^b and Bernhard Rieger^{*a}

Liquid-crystalline compounds with a perfluorinated aromatic ring as the mesogenic core and a propylene carbonate unit were prepared and mixed with lithium bis(trifluoro-methanesulfonyl)-imide (LiTFSI). The self-assembly was driven by the interaction of the polar propylene carbonate unit. Thus it is one of the few examples of liquid crystals with only one phenyl group that is able to self-assemble. Small- and Wide angle X-ray scattering (SAXS/WAXS) measurements indicate that the molecules spontaneously formed a smectic phase. Calculation of the Li-salt dissociation from the data obtained by a combination of impedance spectroscopy measurements and diffusion experiments by ⁷Li and ¹⁹F pulsed field gradient (PFG) NMR revealed good dissociation properties of the compounds. The complex of (2-Oxo-1,3-dioxolan-4-yl)methyl 4-(decyloxy)-2,3,5,6-tetrafluorobenzoate (**4b**) with LiTFSI exhibited anisotropic conductivity. The conductivity parallel to the smectic orientation was 125 times higher than perpendicular and is one of the best reported for liquid crystals with propylene carbonate fragments.

Received 9th October 2014
Accepted 9th December 2014

DOI: 10.1039/c4ta05401f

www.rsc.org/MaterialsA

Introduction

Liquid crystals have gained remarkable attraction as an alternative to common electrolytes like cyclic carbonates and poly(ethylene oxide) (PEO).^{1–3} For the further development of lithium-ion batteries, it is essential to replace the liquid electrolytes by solid ones because they are less flammable and are easily processable.^{4–8} Currently, the most used electrolytes are organic liquids based on linear and cyclic carbonates as their high dielectric constant results in good lithium-ion conductivity.⁹ To overcome the safety problems of organic liquids, Wnek and co-workers synthesized polysiloxanes with cyclic carbonate side chains.¹⁰ Although their polymers have a dielectric constant ranging from 22 to 44, the polymer Li-salt complex has only a conductivity of 5×10^{-7} S cm⁻¹ at room temperature. An alternative could be liquid crystals with cyclic carbonates as the moiety enhancing salt dissociation. Liquid crystals are less flammable and can transport ions efficiently

as segregation leads to the formation of nanoscale ion pathways.^{11–14} Until now, the focus has been mainly on liquid crystals with poly(ethylene oxide) (PEO) moieties.^{15–21} One of the few examples of a liquid crystal with a carbonate fragment was synthesized by Kato and co-workers and it exhibits a hexagonal columnar structure.²² However, the ionic conductivity of 2.2×10^{-8} S cm⁻¹ at 22 °C is relatively low. A reason for the low ionic conductivity could be the high dipole–dipole interactions between the polar cyclic carbonate units.¹⁰ In contrast to molecules with PEO side chains, where the ions are transported through segmental motion of the PEO fragments,²³ carbonates on a polymer backbone show a different conductivity mechanism. The ions are transported *via* diffusion or an ion-hopping mechanism.²⁴ A different molecular structure with a lower molecular weight and a smectic liquid crystalline structure instead of a columnar one can result in an improved ionic conductivity. It is difficult to align columnar structures macroscopically; therefore the ion diffusion is encumbered. Alignment in a smectic structure may enhance ion diffusion through the material.^{11,25} Until now the conductivity mechanism of liquid crystals in the mesogenic phase is not fully understood.

The goal of this work is to synthesize a liquid crystalline molecule with a cyclic carbonate unit which has a good thermal stability and enhanced ionic conductivity when mixed with lithium salts. On the basis of Small- and Wide-Angle X-ray Scattering (SAXS/WAXS), conductivity measurements and diffusion experiments by the PFG-NMR technique, we expect to get a deeper insight into the lithium coordination and the conductivity mechanism of aligned liquid crystals.

^aWACKER-Lehrstuhl für Makromolekulare Chemie, Technische Universität München, Lichtenbergstr. 4, 85747 Garching bei München, Germany. E-mail: rieger@tum.de

^bFachgebiet Physik weicher Materie, Physik Department, Technische Universität München, James-Frank-Str. 1, 85747 Garching bei München, Germany

^cInstitut für Physikalische Chemie, University of Muenster, Corrensstr. 8/30, 48149 Münster, Germany

^dNRW Graduate School of Chemistry, University of Muenster, Wilhelm-Klemm-Str. 10, D-48149 Münster, Germany

† Electronic supplementary information (ESI) available: DSC diagrams for the mixtures of **4a**, **4b** and **4c** with various amounts of LiTFSI; WAXS/SAXS of **4a** and **4b** mixed with 10 mol% LiTFSI, ionic conductivity measurements for **4b**, **6** and **8** with various amounts of LiTFSI; NMR spectra of all compounds discussed in this paper. See DOI: 10.1039/c4ta05401f

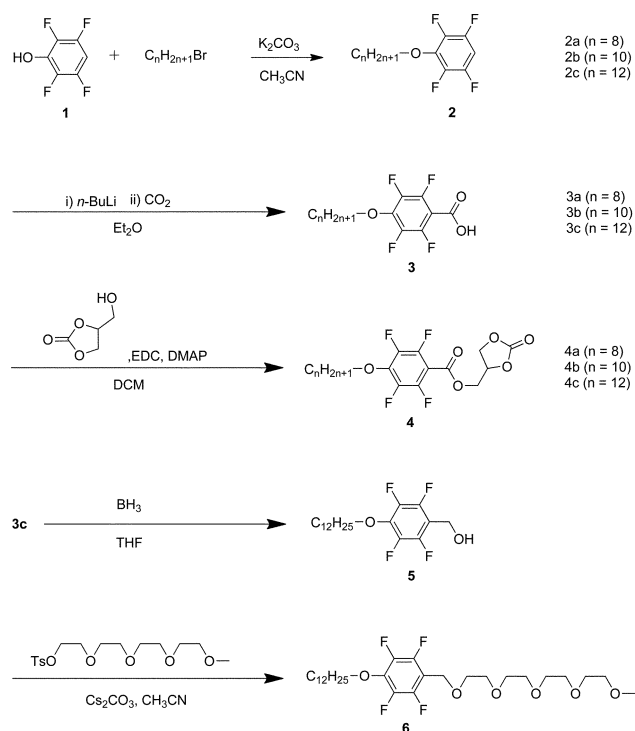
We have chosen a perfluorinated aromatic ring as the mesogenic core, because fluorinated compounds have been found to improve the physical properties in contrast to their hydrocarbon homologues.^{3,26–29} The Li-salt mixtures of the perfluorinated substances may exhibit a higher ionic conductivity compared to their non-fluorinated analogues. In combination with the polar carbonate function, it is possible to synthesize liquid crystalline molecules with a lower molar mass. The higher order in the liquid crystalline state and the cyclic carbonate moiety inducing a high degree of dissociation of the lithium salt may result in enhanced ionic conductivity.^{30,31} The results for the perfluorinated compounds were compared with those for a non-fluorinated molecule. To show the effect of cyclic carbonates on the formation of a liquid crystalline state and the ionic conductivity, also molecules with tetra(ethylene oxide) (TEO) having the same fluorinated mesogenic core were synthesized.

Results and discussion

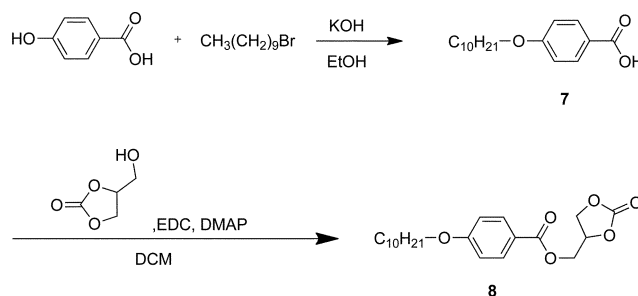
Synthesis of the fluorinated mesogens

The synthesis routes of the fluorinated and non-fluorinated mesogenic molecules which were analyzed in this study are shown in Schemes 1 and 2. Substances **4a**, **4b** and **4c** have a perfluorinated aromatic ring as the mesogenic core and differ in the length of the alkyl chain, whereas **8** has a non-fluorinated mesogenic core.

The syntheses of the mesogenic cores **3** and **7** were carried out according to a modified literature procedure in quantitative yields.^{26,32}



Scheme 1 Synthesis of the investigated fluorinated mesogenic molecules.



Scheme 2 Synthesis of the investigated non-fluorinated mesogenic molecule.

The liquid crystalline compounds **4** and **8** were synthesized by an esterification starting from molecule **3** and **7**, respectively, with glycerine carbonate, EDC and DMAP as coupling agents.²² As the tetrafluorobenzoic acid (**3**) is more reactive than the non-fluorinated benzoic acid used by Kato and co-workers, the amount of the coupling reagents EDC and DMAP could be drastically reduced.

Reduction of **3c** with BH_3 -THF solution (1 M) gave the mesogenic core **5**. BH_3 was chosen as the reduction agent as other reduction agents either led to a partial defluorination of the aromatic ring, mainly on the *meta* position (LiAlH_4) or were too weak (NaBH_4). Compound **6** was synthesized by a standard Williamson ether synthesis in acetonitrile starting from substance **5**.

Thermal properties

The thermal properties of the synthesized compounds were analyzed by differential scanning calorimetry (DSC). Additionally, optical textures of the substances which exhibit a liquid crystalline phase were obtained by polarized optical microscopy (POM).

Fig. 1 presents the DSC traces from the 1st heating scan, the subsequent 2nd heating scans and the subsequent 1st cooling scans obtained for **8**, **4a**, **4b** and **4c**. All compounds, except **6** showed a liquid crystalline phase (see ESI, Fig. S1†). Substance **6** is a liquid at room temperature and crystallizes without the formation of a liquid crystalline state as the intermolecular interaction of the TEO group is too weak. Cyclic carbonates have a higher dipole moment than TEO (propylene carbonate $\mu = 5.36$ D, TEO $\mu = 3.25$ D at 40 °C).^{33,34} Hence the dipole-dipole interaction of the carbonate groups is higher which is expected to increase the interchain interactions.^{10,19,35}

In POM, the formation of a fan-shaped texture was observed for the substances **4b** and **4c** when cooled from the isotropic melt. Substance **4a** formed batonnets and **8** formed a focal conic as well as a fan-shaped texture. These textures are typical for a smectic A (S_A) phase (Fig. 3 and ESI Fig. S15†).³⁶ After further cooling, the compounds started to crystallize, except substance **4a** and **8**, where no crystallization could be observed within the measured temperature range. The longer the alkyl chains of the fluorinated liquid crystalline molecules, the higher are the isotropization temperatures as well as the crystallization temperatures (Fig. 1, Table 1). Compared to **8**, substance **4b** has

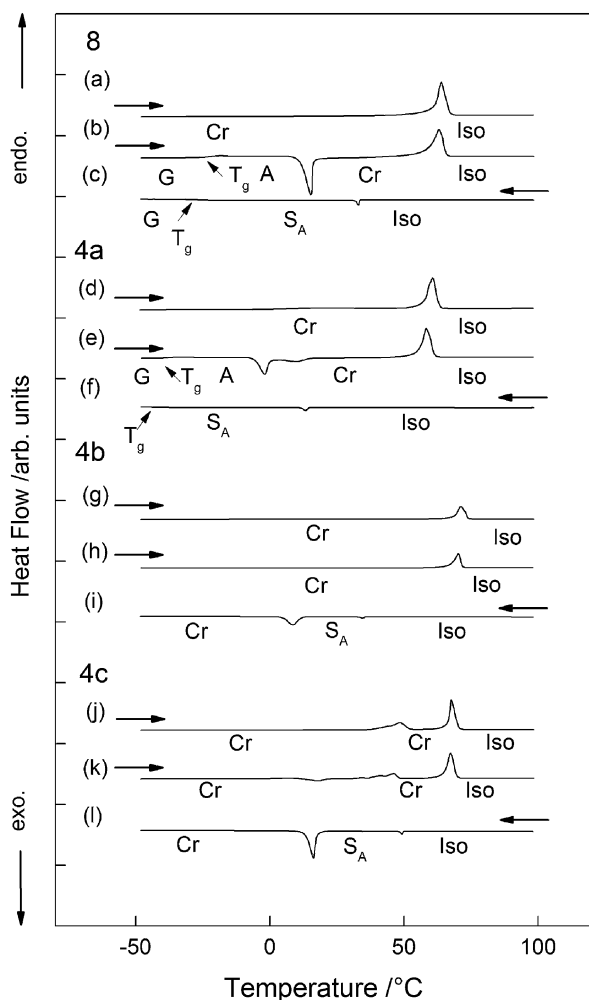


Fig. 1 DSC traces (10 K min^{-1}) of **8**: (a) first heating scan, (b) second and subsequent heating scans, (c) first and subsequent cooling scans; **4a**: (d) first heating scan, (e) second and subsequent heating scans, (f) first and subsequent cooling scans; **4b**: (g) first heating scan, (h) second and subsequent heating scans, (i) first and subsequent cooling scans; **4c**: (j) first heating scan, (k) second and subsequent heating scans, (l) first and subsequent cooling scans. Cr, crystalline; S_A , smectic A; Iso, isotropic; G, glassy; A, amorphous.

a higher isotropization temperature and crystallizes on cooling. This observation suggests that fluorination increases the isotropization temperature and leads to the formation of a crystalline structure. The formation of a liquid crystalline phase for **4a**, **4b**, **4c** and **8** was only observed on the cooling scans, hence the substances have a monotropic mesophase.

Substances **4a**, **4b**, and **4c** were mixed with different amounts of LiTFSI, a common lithium salt, to analyze the influence of the Li salt on the mesomorphic behavior. LiTFSI was chosen as the Li salt because of its good thermal stability and dissociation behavior.⁷ The lithium salt mixtures were obtained by slow evaporation of the THF solution of the substances and LiTFSI. All compounds were solids at room temperature. On cooling from the isotropic melt, the mixtures of **4c** first exhibited a transition into a smectic mesophase, followed by crystallization. This observation was verified by POM. The pictures first showed

Table 1 Thermal transitions of the investigated mesogenic compounds (enthalpy in J g^{-1} in parentheses) detected by DSC from the second heating scan and the first cooling scan

Phase transition ($^{\circ}\text{C}$) and corresponding enthalpy changes ^a (J g^{-1})						
2nd heating						
4a	G	-38	A	-2 (34.5)	Cr	58 (65.2)
4b	Cr	71 (88.8)	I			
4c	Cr	18 (10.8)	Cr	41 (28.1)	Cr	67 (70.9)
8	G	-21	A	16 (61.4)	Cr	64 (89.4)
Cooling						
4a	I	20 (2.5)	S_A	-47	G	
4b	I	37 (2.6)	S_A	13 (53.9)	Cr	
4c	I	49 (2.1)	S_A	16 (63.1)	Cr	
8	I	33 (3.0)	S_A	-23	G	

^a Cr, crystalline; S_A , smectic A; Iso, isotropic; G, glassy; A, amorphous.

a batônnet-like texture followed by the formation of a fan-shaped texture.³⁶

Increasing amounts of LiTFSI broadened the temperature range in the mesogenic phase, see Fig. 2. The highest temperature range was achieved for complex **4b** and **4c** with 20 mol% LiTFSI. Compared to the substances without the Li salt, the temperature range of the mesophase for **4c** increases from 33.3°C up to 82.8°C and for **4b** from 24.6°C up to 97.4°C , respectively (see the ESI, Fig. S3 and S4, and Tables S2 and S3[†]). Up to 10 mol% LiTFSI, the isotropization temperature increased while the crystallization temperature were relatively constant. This is an indication that the Li salt was incorporated into the polar part of the substance. The incorporation of the salt enhances the separation of polar and lipophilic groups, as it makes the polar fragments more polar.^{37,38} Further increase of Li salt concentration leads to the formation of a glassy state, and additionally to a decrease of the crystallization temperature and enthalpy because additional lithium salt disturbs the formation of the crystalline phase. This suggests that higher amounts of

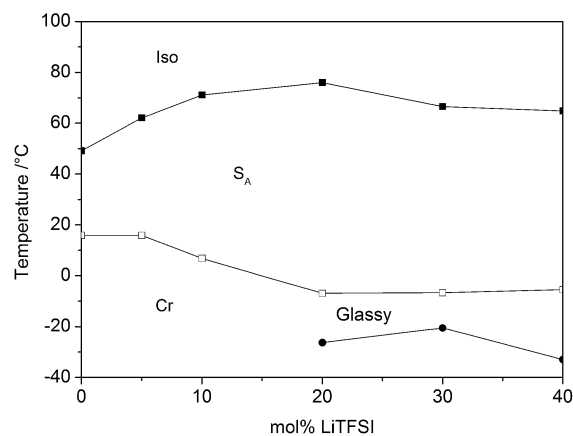


Fig. 2 Phase transition behavior for the mixtures of compound **4c** and LiTFSI, data recorded from the first cooling scans. Iso, isotropic; S_A , smectic A; Cr, crystalline.

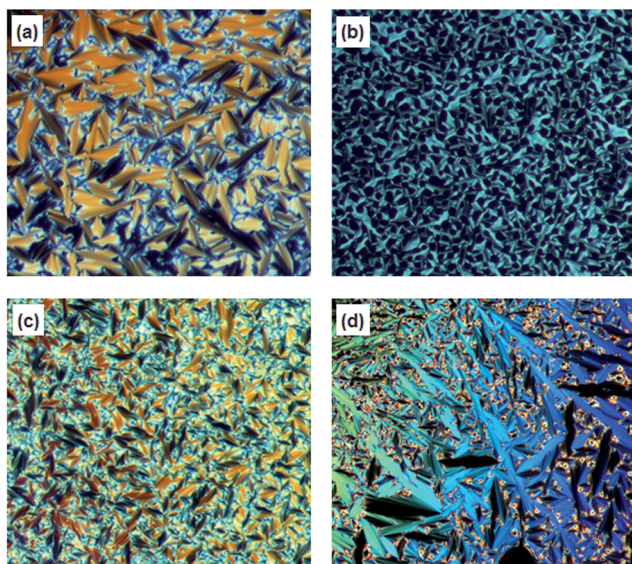


Fig. 3 POM pictures of the synthesized compounds on cooling from the isotropic melt: (a) compound **4b** at 30 °C; (b) substance **4a** at 20 °C; (c) substance **4c** at 45 °C; (d) substance **4c** mixed with 10 mol% LiTFSI at 70 °C.

lithium salt are not only incorporated into the ionic fragments but in all parts of the molecule. Compound **4a** and the salt mixtures exhibited a different thermal behavior. On the cooling scans no crystallization was observed and crystallization occurs on the subsequent 2nd heating scan. The range of the mesogenic phase increased up to 5 mol% LiTFSI. Higher amounts of Li-salt decrease the isotropization temperature and so the range of the liquid crystalline phase. At concentrations higher than 20 mol% LiTFSI no liquid crystalline phase was observed any more. The lithium salts also emphasize the formation of an enantiotropic mesophase. Whereas compound **4c** without and with 5 mol% LiTFSI only has a monotropic mesophase, the compounds with higher amounts of the Li salt exhibit the formation of an enantiotropic mesophase (see the ESI, Fig. S5[†]).^{2,15} This behavior was not observed for substances **4a** and **4b**.

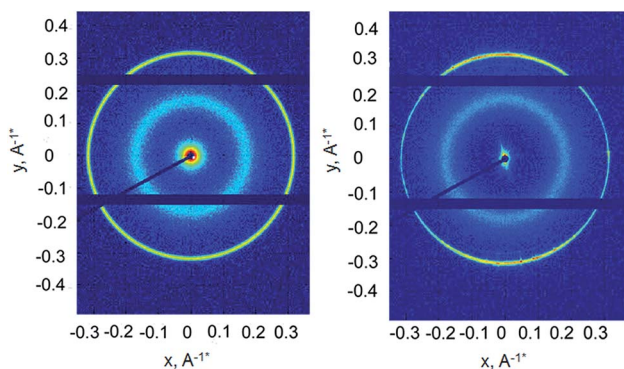


Fig. 4 2D SAXS images of compound **4b** mixed with 10 mol% LiTFSI. Left: not aligned at 40 °C on heating; right: aligned in the S_A phase at 40 °C on cooling from the isotropic temperature. The horizontal stripes of lower intensity are due to the blind regions of the detector.

SAXS and WAXS measurements

SAXS and WAXS experiments were carried out to examine the mesomorphic phase structures of **4a**, **4b**, **4c** and their mixtures with LiTFSI (Fig. 5 and ESI, Fig. S6 and S7[†]). Substances **4a**, **4b** and **4c** and their mixtures with 5 mol% and 10 mol% LiTFSI exhibited a spontaneously macroscopic smectic alignment when the samples were placed between two mica (silica) plates in the measurement cell, heated above the isotropization temperature and subsequently cooled below the isotropic temperature. The concentration of the scattering intensity along the y -axis in the 2D SAXS pattern indicates the aligned smectic layers along the surface of the mica plates in the measurement cell (Fig. 4b). For the non-aligned samples, the diffraction rings are homogeneous (Fig. 4a).³⁵

To show the influence of the lithium salt concentration on the molecular packing arrangement of **4a**, **4b** and **4c**, WAXS/SAXS measurements with different amounts of LiTFSI were performed. At room temperature, all lithium salt mixtures were crystalline, which was confirmed by WAXS measurements. In the WAXS curves the complexes gave sharp reflections (see the ESI, Fig. S8[†]). From the layer spacing and the length of the molecule the d/l ratio can be calculated, see Table 2. The d/l ratio gives an indication about the packing structure of the molecules. A d/l ratio <1 indicates a strongly interdigitated monolayer, whereas ratios of 1–2 indicate the formation of an interdigitated bilayer. The 2D SAXS profiles for **4c** pure and **4c** with 5 mol% LiTFSI exhibit one strong reflection with layer spacing of 21.4 Å and 21.6 Å, respectively, thus the molecules form an interdigitated monolayer (Table 2). Up to 5 mol%, the Li salt has nearly no influence on the layer distances. The compounds with a higher amount of Li salt exhibit two reflections in the SAXS patterns and have a ratio of 1.5 : 1 in the q range which is typical for a bilayered lamellar structure. The formation of a bilayer may be explained by an increased polarity of the ionic group as the Li salt intercalates preferentially into the polar parts of the molecule. This leads to micro-phase segregation between the long alkyl chain and the polar carbonate group. The mixture of **4c** with 10 mol% LiTFSI showed a different SAXS curve (Fig. 5). The first reflection is broader and has a lower intensity than the second reflection. Probably no clear bilayer is formed. Compound **4b** pure and the mixtures with 5 and 10 mol% LiTFSI formed an interdigitated monolayer in a smectic phase. Similar to **4c** small amounts of the lithium salt have nearly no influence on the packing arrangement. The same behavior is also observed for substance **4a**. In **4a** the layers are less interdigitated than in **4b** and **4c**.

The SAXS/WAXS experiments demonstrate that the substances **4a**, **4b** and **4c** and their mixtures with LiTFSI spontaneously align in the smectic phase when they are cooled from the isotropic melt. To show the influence of a magnetic field on the orientation, the compounds **4a** and **4b** mixed with 10 mol% LiTFSI were placed into a magnetic chamber and heated up to the isotropic state. Then a magnetic field with field strength of 9.4 T was applied and the sample was cooled to 20 °C at a rate of 0.5 K min⁻¹. The magnetic field was applied perpendicular to the film surface. After the treatment, the SAXS pattern of **4a**

Table 2 X-ray diffraction analysis and ionic conductivity of compounds **4c**, **4b** and **4a** mixed with various amounts of LiTFSI

Mol% LiTFSI	<i>T</i> (°C)	<i>d</i> ₀₀₁ (Å)	<i>d</i> ₀₀₂ (Å)	Layer spacing (Å)	Molecular length (Å)	Ratio ^a <i>d/l</i>	$\sigma_{i }$ at 55 °C	Phase
4c								
0	40	21.4		21.4	25.9	0.82		Monomolecular S _A
5	45	21.6		21.6	25.9	0.83	1.9×10^{-5}	Monomolecular S _A
10	50	35.9	22.1	35.9	25.9	1.38	2.0×10^{-5}	Bimolecular S _A
20	40	37.6	18.9	37.6	25.9	1.45	2.1×10^{-5}	Bimolecular S _A
40	40	39.0	19.4	39.0	25.9	1.50	2.0×10^{-5}	Bimolecular S _A
4b								
0	25	19.6		19.6	24.7	0.79		Monomolecular S _A
5	40	19.9		19.9	24.7	0.81	1.8×10^{-5}	Monomolecular S _A
10	40	20.1		20.1	24.7	0.81	2.9×10^{-5}	Monomolecular S _A
4a								
0	20	18.5		18.5	21.0	0.88		Monomolecular S _A
10	20	18.4		18.4	21.0	0.88	2.1×10^{-6b}	Monomolecular S _A

^a Ratio of layer spacing, *d*, to the molecular length, *l*. ^b $\sigma_{i||}$ at 20 °C.

shows a large number of diffraction spots, which is an indication that the smectic layer plane is now oriented perpendicular to the surface of the mica plates (see the ESI, Fig. S13†). The smectic layer plane is oriented along the direction of the magnetic field, which shows that the alignment is influenced by external fields. The same behavior was observed for **4b**.

Conductivity measurements

Temperature dependent ionic conductivities were measured for the LiTFSI mixtures of **4a**, **4b**, **4c**, **6** and **8** by an alternating current impedance method on cooling with two different cells. Cell A is an IDA electrode (Interdigitated Array) purchased at ALS, Japan. With risograph technology, a micro-pattern is formed on an isolated glass plate to allow the electric field to be applied parallel to the substrate surface. To enhance the alignment of the smectic layer planes in the liquid crystalline state, the sample was covered with a glass plate when the

temperature was above the isotropic point. Cell B consists of a pair of indium tin oxide (ITO) electrodes. The thickness between the electrodes was 250 μm, and they were fixed with a Teflon spacer. The LiTFSI mixtures were placed on the electrodes and heated above the isotropic point and the ionic conductivity was then measured on cooling to room temperature.^{39,40}

As shown above (Fig. 4) the substances **4a**, **4b** and **4c** and their mixtures with LiTFSI align in the smectic phase when they are cooled from the isotropic melt. This behavior leads to anisotropic conductivity. In cell A where the current is applied parallel to the surface, compound **4b** mixed with 10 mol% LiTFSI showed an alignment of the smectic layers parallel to the surface, when cooled from the isotropic melt. The conductivity was measured parallel to the film surface (*x*- and *y*-direction) ($\sigma_{i||}$) (Fig. 6). In cell B the conductivity was measured perpendicular to the film surface (*z*-direction, $\sigma_{i\perp}$). POM pictures of **4b** in cell B showed the formation of a fan-shaped texture (see the ESI, Fig. S14†) which indicates the formation of polydomains and thus no macroscopic orientation. The ionic conductivity ($\sigma_{i\perp}$) decreased to 1.2×10^{-7} S cm⁻¹ at 45 °C on cooling (Fig. 7) as migration of the cations was hindered on the built grain boundaries and was 125 times lower than in cell A ($\sigma_{i||} = 1.5 \times 10^{-5}$ S cm⁻¹ at 45 °C). The highest conductivity was achieved for **4a** mixed with 10 mol% LiTFSI in cell A. As the smectic transition occurs only at 18 °C, the molecules do not align in the measurement cell till 20 °C and the conductivity in cell A and cell B is almost the same. Below 20 °C a small decline of the conductivity is observed in cell B, which indicates an alignment of the molecules parallel to the surface of the cell, hence perpendicular to the measured conductivity (Fig. 7).⁴¹ The ionic conductivity for **4a** and **4b** in cell A is significantly higher than the conductivity observed by Kato and co-workers for a similar molecule with a cyclic carbonate unit which aligned in a columnar phase.²² This observation suggests that molecules with a similar structure exhibit in a layered phase a higher

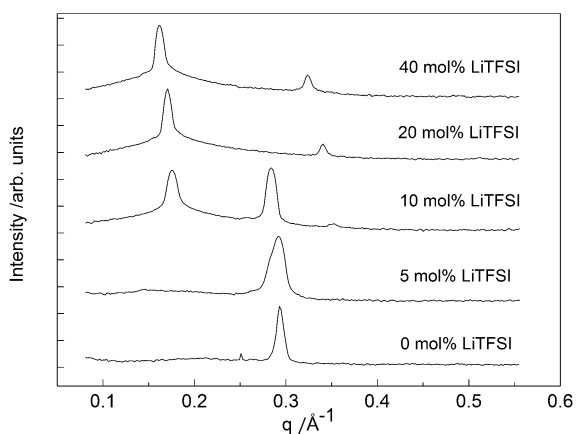


Fig. 5 SAXS curves of compound **4c** with various amounts of LiTFSI. The curves were shifted vertically for clarity.

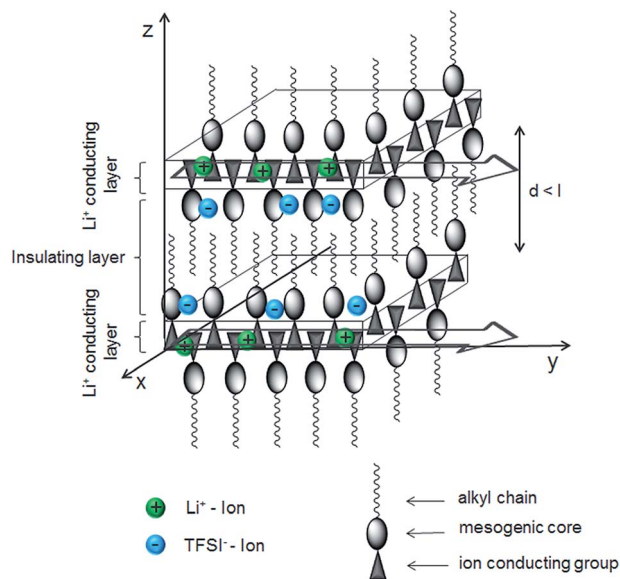


Fig. 6 Schematic illustration of anisotropic Li^+ ion conductivity along the layer plane in x - and y -direction when the molecules align in an oriented interdigitated monomolecular S_A phase.

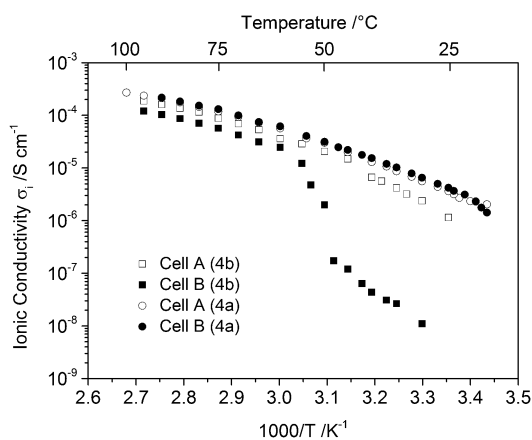


Fig. 7 Arrhenius plots of ionic conductivity for **4a** and **4b** with 10 mol% LiTFSI; measured parallel (cell A, σ_{\parallel}) and perpendicular (cell B, σ_{\perp}) to the smectic layer plane of the aligned liquid crystals, respectively.

conductivity than in the columnar phase. Probably, the ion transport mechanism is hindered in a 1D structure if there is no perfect macroscopic alignment such that the ion channels are interrupted and agglomeration between the Li-salt and the polar coordination sites may be favored. The LiTFSI mixture of substance **8**, the non-fluorinated analogue of **4b** exhibited a significantly lower conductivity. Additionally no alignment could be observed in the measurement cell; hence the ionic conductivity is almost the same in both measurement cells (see the ESI, Fig. S12[†]). These results indicate that fluorination has a positive effect on both the alignment in the measurement cell and the ionic conductivity.

Compounds **4b** and **4c** were mixed with different amounts of LiTFSI. The best ionic conductivity was achieved for the

compounds with 10 mol% LiTFSI per carbonate unit. Higher amounts of Li salt had nearly no influence on the ionic conductivity, although they had an influence on the intermolecular structure, as shown above (Table 2). According to eqn (1) ionic conductivity depends on the concentration, n_+ , of the cationic charge carriers as well as on their mobility, μ_+ .

$$\sigma = Fn_+\mu_+ \quad (1)$$

where F is the Faraday constant. At higher concentrations the number of cationic charge carriers increases, but their mobility is hindered due to the formation of aggregates.^{42–44} As in solid electrolytes with carbonate units there is no segmental motion like in electrolytes with PEG chains; the mobility of the ions only depends on the potential barrier, E_{hop} , that the cation must overcome to move from one site to another. Increasing ion concentration leads to the formation of ion aggregates which increases this energy barrier.⁴¹ The reduced intensity of the ^7Li signal in the NMR spectra also indicates the formation of molecular aggregates (see ESI, Fig. S17[†]). A different behavior is observed for compound **6**, which behaves more like a liquid electrolyte where diffusion in a liquid is expected to be isotropic. Here, increasing amounts of LiTFSI increase the ionic conductivity (see ESI, Fig. S10[†]).

As expected the conductivity in the isotropic phase mainly depends on the length of the alkyl chain. The shorter the alkyl chain, the lower the molecular mass and the higher is the ionic conductivity (see ESI, Fig. S9[†]). Furthermore, fluorination of the aromatic core has a positive effect on the ionic conductivity. Hence, substance **4a** has with $2.7 \times 10^{-4} \text{ S cm}^{-1}$ at 100 °C the highest conductivity of all measured compounds.

Diffusion behavior and salt dissociation

The self-diffusion coefficients of both the cation and the anion species in the LiTFSI mixtures for **4a**, **4b** and **6** were measured by the PFG-NMR technique. After heating up to 80 °C the diffusion was measured during cooling. Density, molar mass and molar salt concentration C , which were used for the calculations, are compiled in Table S4 (see the ESI[†]). Because of the lower molecular weight of **4a**, the substance contains a higher molar salt concentration. As described above, the salt concentration has only a minor effect on the conductivity.

Table 3 shows the diffusion coefficients, conductivity and the calculated Haven ratios for the substances **4a**, **4b** and **6** with 10 mol% LiTFSI. When both the conductivity and the diffusion data are known, the calculation of the Haven ratio, $A_{\text{imp}}/A_{\text{NMR}}$ is a good approach to estimate the dissociation behavior of the Li salt in the liquid crystalline matrix. The calculation of the Haven ratio was done according to the approach by Kii and co-workers.^{45,46} The molar conductivity A_{imp} was calculated from the ionic conductivity σ_i obtained from impedance measurements by the following equation

$$A_{\text{imp}} = \frac{\sigma_i}{C} \quad (2)$$

Table 3 Diffusion coefficients of the cation and anion at different temperatures. Ionic conductivity and calculated Haven ratio $A_{\text{imp}}/A_{\text{NMR}}$ for **4a**, **4b** and **6** with 10 mol% LiTFSI in the isotropic phase

Compound	T ($^{\circ}\text{C}$)	D_{Li} ($\text{cm}^2 \text{s}^{-1}$)	D_{F} ($\text{cm}^2 \text{s}^{-1}$)	σ_i (S cm^{-1})	$A_{\text{imp}}/A_{\text{NMR}}$
4a /10 mol% LiTFSI	80	1.3×10^{-7}	1.8×10^{-7}	1.5×10^{-4}	0.52
	55	2.3×10^{-8}	4.2×10^{-8}		
	40	7.8×10^{-9}	9.7×10^{-9}		
4b /10 mol% LiTFSI	80	1.7×10^{-7}	2.4×10^{-7}	1.2×10^{-4}	0.33
	55	1.8×10^{-8}	3.1×10^{-8}		
6 /10 mol% LiTFSI	55	4.5×10^{-7}	7.9×10^{-7}	1.1×10^{-5}	0.01
	30	7.9×10^{-8}	1.5×10^{-7}		

Using the diffusion coefficients D_{Li} and D_{F} from the NMR measurements the molar conductivity A_{NMR} can be calculated by applying the Nernst–Einstein relationship for univalent electrolytes.

$$A_{\text{NMR}} = \frac{F^2}{RT} (D_{\text{Li}} + D_{\text{F}}) \quad (3)$$

where F is the Faraday constant.⁴⁷ A_{NMR} calculated from the diffusion measurements is usually higher than A_{imp} as the value includes the diffusivity of the dissociated ions as well as that of the ion pairs.⁴⁸

As expected, the diffusion coefficients decrease with decreasing temperature and show for all substances strong temperature dependence. While this trend is a general consequence of diffusion resulting from thermally activated ion jumps, in the present case the phase transitions as well as the alignment of the smectic layers might play a role. The magnetic field orientation was parallel to the direction of the magnetic field gradients; thus, in the oriented smectic phases, the diffusion is measured parallel to the smectic layer plane. Between 80 $^{\circ}\text{C}$ and 55 $^{\circ}\text{C}$, the diffusion coefficient of **4b** decreases stronger (factors of 9 and 8 for ^7Li and ^{19}F , respectively) than that of **4a** (factors of 6 and 4, respectively). Knowing that **4b** is in the smectic phase and **4a** is in the isotropic phase at 55 $^{\circ}\text{C}$ (see also Fig. 7), and assuming an at least partial orientation of the smectic layers of **4b** in the magnetic field, it would imply that the net effect of the formation of smectic layers and their orientation leads to a lower diffusivity of the ions. This seems surprising, but might be an effect of a strong binding of Li (and thus also anions by contact ion pairs) to the high concentration of carbonates in the conductive, polar region. Another reason might be a not ideal orientation in the field, such that polydomains are formed and migration is hindered by the formed grain boundaries.

The diffusion coefficient of Li^+ is generally lower than that of the anions. This reveals that Li^+ is more affected by the polar sites of the molecules. Li^+ interacts with the oxygen of the carbonate units *via* coordination to free electron pairs of oxygen and tends to hop from site to site through the liquid crystalline matrix. The ratio of Li and F diffusion coefficients is in the range between 0.5 and 0.8 without any systematic dependencies. It reflects the fact that the anion is generally faster, but its diffusivity is correlated to that of the cation. Most probably there are contact ion pairs formed, such that Li^+ and the anion partially

diffuse in a correlated fashion, as was shown for Li salt-in-polymer electrolytes.⁴⁹ As the anion is not affected by coordination it exhibited a higher diffusion coefficient at lower temperature. This is in accordance with the results for polymer gel electrolytes based on poly(ethylene glycol).^{35,41–44}

Most interesting, however, are the Haven ratios, as they reach quite high values. Cyclic carbonates have a high dielectric constant; therefore the polar sites on the liquid crystalline molecules **4a** and **4b** promoted salt dissociation and the Haven ratio is significantly higher than for liquid crystalline molecules with other polar groups and is higher than for molecule **6** with a TEO unit (Table 3).⁵⁰ Though the correlation of Li^+ and anion motion is certainly still present, it is less pronounced as compared to these materials. Since the Haven ratio depends on the orientation of the smectic layers, it was only determined in the isotropic state.

Conclusions

Liquid crystalline substances with a propylene carbonate unit as the ionically conductive group were prepared. It was shown that carbonate units enhance the formation of a liquid crystalline state. SAXS/WAXS measurements demonstrated that the molecules align spontaneously in the smectic phase when they are cooled from the isotropic melt. The LiTFSI mixtures of **4a** and **4b** aligned in the measurement cells and anisotropic conductivity could be observed. Fluorination of the aromatic ring significantly increases the ionic conductivity of the Li-salt mixtures. Determination of the diffusion coefficients and calculation of the Haven ratio revealed that the cyclic carbonate moiety on the molecules enhanced Li-salt dissociation compared to the molecules containing a TEO unit and the Li cation was probably transported by a hopping mechanism through the liquid crystalline matrix. The formation of a smectic layer enhances ion mobility parallel to the layer plane which enhances the ionic conductivity. Therefore one of the best ionic conductivities for liquid crystalline molecules with cyclic carbonate units could be achieved.

Experimental section

Materials

Unless otherwise noted the reagents and solvents were purchased from Aldrich, ABCR, Alfa Aesar and Gruesing. The

dry solvents were taken from a solvent-purification-system MB SPS-800 from MBraun.

Characterization

^1H NMR spectra were measured on an AVIII-300 from Bruker at 300 K and at 300 MHz. Chemical shifts were quoted relative to $(\text{CH}_3)_4\text{Si}$ ($\delta = 0.00$) as an internal standard or to the residual protons of the deuterated solvents. The multiplicity was characterized by the following abbreviations: s – singlet, d – doublet, t – triplet, q – quartet, p – quintet, m – multiplet. ^{19}F NMR spectra were recorded on a Bruker AV-250 at 300 K and 250 MHz.

IR measurements were conducted using a Bruker Vertex 70 FT/IR with an ATR unit. Electrospray ionization mass spectrometry (ESI-MS) was performed on a Varian 500 MS.

Differential scanning calorimetry (DSC)

DSC measurements were performed on a Q 2000 from TA Instruments. Heating and cooling rates were 10 K min^{-1} . The transition temperatures were taken at the maximum of exothermic and minimum point of endothermic peaks, respectively.

Polarized optical microscopy (POM)

POM was done on a Leica MZ8 optical microscope equipped with a Mettler FP52 hot stage.

Ionic conductivity measurements

Electronic impedance spectroscopy (EIS) was carried out on a BioLogic Science Instruments VMP3 potentiostat (frequency range 20 Hz to 500 kHz) and a custom setup temperature controller. Analysis of the data was done with a BioLogic EC-Lab. Sample preparation and the measurements were performed in a glove box under an argon atmosphere. For the conductivity measurements of the liquid crystals, two different electrodes were used. An IDA electrode (Interdigitated Array) purchased at ALS, Japan (cell constant: 0.07 cm^{-1}) and a home-made ITO electrode (cell constant: 0.19 cm^{-1}).

Small- and wide-angle X-ray scattering (SAXS/WAXS)

SAXS/WAXS measurements were carried out using a Ganesha 300XL SAXS–WAXS system (SAXSLAB ApS, Copenhagen/Denmark). The X-ray source was a GENIX 3D microfocuss X-ray source which was operated at 50 kV/0.6 mA with a Cu anode (K_{α} , $\lambda = 0.1542\text{ nm}$). A movable two-dimensional (2D) Pilatus 300K detector was used. All measurements were performed in a fully evacuated chamber. To measure the structural changes, the samples were placed between two mica sheets (5–7 μm thickness). They were heated above the isotropization temperatures and then cooled down with a rate of 10 K min^{-1} . Sample-detector-distances (SDD) of 101 mm (WAXS) and 401 mm (SAXS) were used, resulting in a q -range of 0.01 to 2.5 \AA^{-1} (q is the momentum transfer). The 2D images obtained were azimuthally averaged. The layer spacing was determined from a

Lorentzian fit from the first-order Bragg reflection with the Bragg relationship $d = 2\pi/q_0$.

Pulsed field gradient NMR studies

Diffusion coefficients of the ionic species in the electrolytes were measured using the pulsed gradient stimulated echo (PGF) NMR technique on a Bruker 400 MHz FT-NMR spectrometer (Bruker, Avance) employing a probe head (Bruker, DIF3 30) with RF-selective inserts for the respective nuclei and providing magnetic field gradient strength of up to 12 T m^{-1} . For the measurements, the electrolytes were filled in 5 mm NMR tubes, which were sealed. A stimulated echo pulse sequence was used for the measurements. Gradient pulses of a duration of $\delta = 1.9$ – 2.5 ms and an observation time of $\Delta = 200\text{ ms}$ for ^{19}F and $\Delta = 150\text{ ms}$, $\delta = 2.5\text{ ms}$ for ^7Li experiments, respectively, were applied. The evaluation of the self-diffusion coefficients of TFSI^- and Li^+ was carried out by analyzing the area of the peak of ^{19}F and ^7Li , respectively. The decay of the signal in dependence of the gradient strength g resulted in the diffusion coefficient by fitting the Stejskal–Tanner equation.^{51–54} The gradient pulses were applied in the direction of the magnetic field, B_0 .

Synthesis

General procedure for the synthesis of 4-(alkoxy)-2,3,5,6-tetrafluorobenzene (2a, 2b, 2c). In a round bottom flask fitted with a reflux condenser, a nitrogen inlet and a magnetic stirrer were placed 2,3,5,6-tetrafluorophenol (50.0 mmol, 1.0 eq.), anhydrous potassium carbonate (75.0 mmol, 1.5 eq.) and acetonitrile (80 mL). Under stirring, the reaction mixture was heated to reflux (oil bath, $T = 85\text{ }^\circ\text{C}$). Once reflux was reached, bromoalkane (52.5 mmol, 1.1 eq.) was slowly added with a syringe over 10 min. Then, the reaction mixture was stirred under reflux for 16 h. After cooling the mixture to room temperature, water (200 mL) was added and the aqueous phase was extracted with petroleum ether ($4 \times 100\text{ mL}$). The organic layer was washed with NaOH (10%, 200 mL), neutralized with water and dried over Na_2SO_4 . Evaporation of the solvent with a rotary vapor led to a clear, pale yellow oil in high yields. The substance was used without further purification.

4-(Octyloxy)-2,3,5,6-tetrafluorobenzene (2a). Yield 98%. ^1H -NMR (300 MHz, CDCl_3 , 300 K) δ (ppm) = 0.89 (t, $^3J = 6.71\text{ Hz}$, 3H), 1.30 (m, 8H), 1.46 (p, $^3J = 6.96\text{ Hz}$, 2H), 1.78 (p, $^3J = 6.65\text{ Hz}$, 2H), 4.22 (t, $^3J = 6.57\text{ Hz}$, 2H), 6.75 (m, 1H). ^{13}C -NMR (63 MHz, CDCl_3 , 300 K) δ (ppm) = 13.77 (1C), 22.39 (1C), 25.28 (1C), 26.67 (1C), 28.64 (1C), 29.64 (1C), 31.53 (1C), 75.11 (1C), 98.88 (1C), 138.34–138.71 (1C), 139.59–139.88 (1C), 142.85–143.09 (1C), 144.85 (1C), 148.17 (1C). ^{19}F -NMR (235 MHz, CDCl_3 , 300 K) δ (ppm) = -157.30 (m, 1F), -157.24 (m, 1F), -140.46 (m, 1F), -140.41 (m, 1F).

4-(Decyloxy)-2,3,5,6-tetrafluorobenzene (2b). Yield 97%. ^1H -NMR (300 MHz, CDCl_3 , 300 K) δ (ppm) = 0.88 (t, $^3J = 6.71\text{ Hz}$, 3H), 1.27 (m, 12H), 1.46 (p, $^3J = 6.96\text{ Hz}$, 2H), 1.79 (p, $^3J = 6.65\text{ Hz}$, 2H), 4.22 (t, $^3J = 6.57\text{ Hz}$, 2H), 6.75 (m, 1H). ^{13}C -NMR (63 MHz, CDCl_3 , 300 K) δ (ppm) = 14.23 (1C), 22.87 (1C), 25.71 (1C), 29.44 (1C), 29.51 (1C), 29.72 (2C), 30.06 (1C), 32.09 (1C), 75.41–75.52 (1C), 99.39 (1C), 138.27–138.70 (1C), 139.52–139.82 (1C),

142.79–143.16 (1C), 144.84 (1C), 148.12 (1C). ^{19}F -NMR (235 MHz, CDCl_3 , 300 K) δ (ppm) = -157.33 (m, 1F), -157.20 (m, 1F), -140.50 (m, 1F), -140.37 (m, 1F).

4-(Dodecyloxy)-2,3,5,6-tetrafluorobenzene (2c). Yield 98%. ^1H -NMR (300 MHz, CDCl_3 , 300 K) δ (ppm) = 0.88 (t, $^3J = 6.71$ Hz, 3H), 1.26 (m, 16H), 1.44 (p, $^3J = 6.96$ Hz, 2H), 1.77 (p, $^3J = 6.65$ Hz, 2H), 4.21 (t, $^3J = 6.57$ Hz, 2H), 6.75 (m, 1H). ^{13}C -NMR (63 MHz, CDCl_3 , 300 K) δ (ppm) = 14.27 (1C), 22.85 (1C), 25.69 (1C), 29.40 (1C), 29.51 (1C), 29.68 (1C), 29.72 (1C), 29.79 (2C), 30.04 (1C), 32.08 (1C), 75.49 (1C), 99.32 (1C), 138.34–138.71 (1C), 139.60–139.81 (1C), 142.86–143.06 (1C), 144.81 (1C), 148.08 (1C). ^{19}F -NMR (235 MHz, CDCl_3 , 300 K) δ (ppm) = -157.16 (m, 1F), -157.11 (m, 1F), -140.27 (m, 1F), -140.32 (m, 1F).

General procedure for the synthesis of 4-(alkoxy)-2,3,5,6-tetrafluorobenzoic acid (3a, 3b, 3c). Compound 2 (67.4 mmol, 1.0 eq.) was dissolved in dry diethyl ether (200 mL) in a dried and argon filled three necked flask and cooled to -70°C in an acetone/dry ice bath. Then, *n*-butyl lithium (2.5 M in hexane) (67.4 mmol, 1.0 eq.) was added, and the reaction mixture was stirred for 3 h at this temperature. Dried CO_2 was then bubbled through the mixture for about 30 min at -70°C . Under continuous CO_2 bubbling, the mixture was allowed to warm to room temperature. The solvent was removed; the crude product was dissolved in water and acidified with HCl (1 N) to bring the solution to $\text{pH} \approx 2$. The mixture was extracted with diethyl ether, pre-dried with brine and dried over Na_2SO_4 . Evaporation of the solvent with a rotary vapor led to a white-yellow solid. The crude product was purified by recrystallization in cyclohexane yielding the final product as a white solid.

4-(Octyloxy)-2,3,5,6-tetrafluorobenzoic acid (3a). Yield 57%. ^1H -NMR (300 MHz, CDCl_3 , 300 K) δ (ppm) = 0.89 (t, $^3J = 6.74$ Hz, 3H), 1.31 (m, 8H), 1.43 (p, $^3J = 6.84$ Hz, 2H), 1.80 (p, $^3J = 6.61$ Hz, 2H), 4.37 (t, $^3J = 6.54$ Hz, 2H), 10.61 (s, 1H). ^{13}C -NMR (63 MHz, CDCl_3 , 300 K) δ (ppm) = 14.24 (1C), 22.79 (1C), 25.59 (1C), 29.30 (2C), 30.01 (1C), 31.90 (1C), 75.52 (1C), 103.61 (1C), 139.07–139.33 (1C), 141.91 (1C), 142.31–142.62 (1C), 144.95–145.22 (1C), 148.43–148.84 (1C), 165.29 (1C). ^{19}F -NMR (235 MHz, CDCl_3 , 300 K) δ (ppm) = -156.67 (m, 1F), -156.62 (m, 1F), -138.23 (m, 1F), -138.17 (m, 1F).

4-(Decyloxy)-2,3,5,6-tetrafluorobenzoic acid (3b). Yield 88%. ^1H -NMR (300 MHz, CDCl_3 , 300 K) δ (ppm) = 0.88 (t, $^3J = 6.74$ Hz, 3H), 1.27 (m, 12H), 1.46 (p, $^3J = 6.84$ Hz), 1.80 (p, $^3J = 6.65$ Hz), 4.37 (t, $^3J = 6.44$ Hz, 2H), 9.56 (s, 1H). ^{13}C -NMR (63 MHz, CDCl_3 , 300 K) δ (ppm) = 14.12 (1C), 22.70 (1C), 25.45 (1C), 29.20 (1C), 29.32 (1C), 29.57 (2C), 29.87 (1C), 31.90 (1C), 75.38 (1C), 103.49 (1C), 138.88–139.14 (1C), 141.77 (1C), 142.22–142.48 (1C), 144.86–145.17 (1C), 148.30–148.86 (1C), 165.80 (1C). ^{19}F -NMR (235 MHz, CDCl_3 , 300 K) δ (ppm) = -156.69 (m, 1F), -156.64 (m, 1F), -138.24 (m, 1F), -138.19 (m, 1F).

4-(Dodecyloxy)-2,3,5,6-tetrafluorobenzoic acid (3c). Yield 95%. ^1H -NMR (300 MHz, CDCl_3 , 300 K) δ (ppm) = 0.88 (t, $^3J = 6.74$ Hz, 3H), 1.26 (m, 16H), 1.46 (p, $^3J = 6.84$ Hz, 2H), 1.80 (p, $^3J = 6.64$ Hz, 2H), 4.37 (t, $^3J = 6.54$ Hz, 2H), 11.42 (s, 1H). ^{13}C -NMR (63 MHz, CDCl_3 , 300 K) δ (ppm) = 14.26 (1C), 22.85 (1C), 25.61 (1C), 29.34 (1C), 29.50 (1C), 29.64 (1C), 29.70 (1C), 29.78 (2C), 30.03 (1C), 32.07 (1C), 75.55 (1C), 103.64 (1C), 139.05–139.36 (1C), 141.90 (1C), 142.39–142.60 (1C), 145.04–145.30 (1C),

148.51–148.75 (1C), 165.60 (1C). ^{19}F -NMR (235 MHz, CDCl_3 , 300 K) δ (ppm) = -156.68 (m, 1F), -156.53 (m, 1F), -138.30 (m, 1F), -138.13 (m, 1F).

General procedure for the synthesis of (2-oxo-1,3-dioxolan-4-yl)methyl 4-(alkoxy)-2,3,5,6-tetrafluorobenzoate (4a, 4b, 4c). To a solution of 1-ethyl-3-(3-dimethylaminopropyl) carbodiimide hydrochloride (EDC) (24.2 mmol, 1.1 eq.) and 4-dimethylaminopyridine (DMAP) (24.2 mmol, 1.1 eq.) in dry DCM (140 mL) 4-(alkoxy)-2,3,5,6-tetrafluorobenzoic acid (3) (22.0 mmol, 1.0 eq.) was added under cooling with ice/water and stirred for one hour. Then, glycerol 1,2-carbonate (44.0 mmol, 2.0 eq.) was added, and the mixture was stirred for 2 days at room temperature. The reaction mixture was then poured into a saturated NH_4Cl aqueous solution, the organic phase was separated and the aqueous phase was extracted with CH_2Cl_2 . The organic phase was pre-dried with brine and dried over Na_2SO_4 . The solvent was evaporated *in vacuo* and the crude product purified by column chromatography (eluent: DCM – $\text{MeOH} = 95/5$) to obtain the product as a viscous liquid which started to crystallize after several minutes to a white solid.

(2-Oxo-1,3-dioxolan-4-yl)methyl 4-(octyloxy)-2,3,5,6-tetrafluorobenzoate (4a). Yield 55%. ^1H -NMR (300 MHz, CDCl_3 , 300 K) δ (ppm) = 0.88 (t, $^3J = 6.69$ Hz, 3H), 1.30 (m, 8H), 1.45 (p, $^3J = 6.86$ Hz, 2H), 1.79 (p, $^3J = 6.59$ Hz, 2H), 4.35 (t, $^3J = 6.54$ Hz, 2H), 4.40–4.51 (m, 2H), 4.60–4.71 (m, 2H), 5.01 (m, 1H). ^{13}C -NMR (75 MHz, CDCl_3 , 295 K) δ (ppm) = 14.14 (1C), 22.70 (1C), 25.50 (1C), 29.21 (2C), 29.92 (1C), 31.81 (1C), 62.23 (1C), 65.91 (1C), 73.43 (1C), 75.50 (1C), 103.59 (1C), 139.69–139.88 (1C), 141.49–141.86 (2C), 145.21–145.40 (1C), 147.26–147.42 (1C), 154.44 (1C), 159.41 (1C). ^{19}F -NMR (235 MHz, CDCl_3 , 300 K) δ (ppm) = -156.22 (m, 1F), -156.16 (m, 1F), -139.23 (m, 1F), -139.17 (m, 1F). IR (ATR): $\nu = 2919, 2853, 1800, 1780, 1731, 1645, 1505, 1486, 1405, 1384, 1314, 1211, 1183, 1091, 1051, 1006, 850, 776, 713$. ESI-MS (m/z): [M^+] calculated for $\text{C}_{19}\text{H}_{22}\text{F}_4\text{O}_6$, 422.4; found, 445.4 ([$\text{M} + \text{Na}^+$]). EA (%) calculated: C 54.03, H 5.25, F 17.99, O 22.73. Found: C 54.05, H 5.52, F 17.70.

(2-Oxo-1,3-dioxolan-4-yl)methyl 4-(decyloxy)-2,3,5,6-tetrafluorobenzoate (4b). Yield 58%. ^1H -NMR (300 MHz, CDCl_3 , 300 K) δ (ppm) = 0.86 (t, $^3J = 6.67$ Hz, 3H), 1.26 (m, 12H), 1.44 (p, $^3J = 6.86$ Hz, 2H), 1.78 (p, $^3J = 6.60$ Hz, 2H), 4.34 (t, $^3J = 6.54$ Hz, 2H), 4.40–4.47 (m, 2H), 4.59–4.70 (m, 2H), 5.03 (m, 1H). ^{13}C -NMR (75 MHz, CDCl_3 , 295 K) δ (ppm) = 14.25 (1C), 22.81 (1C), 25.56 (1C), 29.30 (1C), 29.42 (1C), 29.62 (2C), 29.88 (1C), 32.00 (1C), 64.21 (1C), 65.91 (1C), 73.31 (1C), 75.52 (1C), 103.59 (1C), 139.71–139.86 (1C), 141.52–141.87 (2C), 145.23–145.42 (1C), 147.28–147.47 (1C), 154.41 (1C), 159.43 (1C). ^{19}F -NMR (235 MHz, CDCl_3 , 300 K) δ (ppm) = -156.17 (m, 1F), -156.12 (m, 1F), -139.19 (m, 1F), -139.13 (m, 1F). IR (ATR): $\nu = 2919, 2852, 1800, 1780, 1731, 1644, 1504, 1486, 1405, 1384, 1314, 1211, 1183, 1091, 1050, 1004, 850, 776, 715$. ESI-MS (m/z): [M^+] calculated for $\text{C}_{21}\text{H}_{26}\text{F}_4\text{O}_6$, 450.4; found, 473.4 ([$\text{M} + \text{Na}^+$]). EA (%) calculated: C 56.00, H 5.82, F 16.87, O 21.31. Found: C 56.06, H 5.97, F 16.80.

(2-Oxo-1,3-dioxolan-4-yl)methyl 4-(dodecyloxy)-2,3,5,6-tetrafluorobenzoate (4c). Yield 63%. ^1H -NMR (300 MHz, CDCl_3 , 300 K) δ (ppm) = 0.87 (t, $^3J = 6.69$ Hz, 3H), 1.25 (m, 16H), 1.44 (p, $^3J = 6.86$ Hz, 2H), 1.78 (p, $^3J = 6.59$ Hz, 2H), 4.35 (t, $^3J = 6.54$ Hz,

2H), 4.41–4.70 (m, 4H), 5.05 (m, 1H). $^{13}\text{C-NMR}$ (75 MHz, CDCl_3 , 295 K) δ (ppm) = 14.23 (1C), 22.81 (1C), 25.56 (1C), 29.30 (1C), 29.46 (1C), 29.60 (1C), 29.66 (1C), 29.74 (2C), 29.97 (1C), 32.03 (1C), 64.22 (1C), 65.92 (1C), 73.35 (1C), 75.54 (1C), 103.60 (1C), 139.71–139.86 (1C), 141.52–141.87 (2C), 145.25–145.44 (1C), 147.30–147.49 (1C), 154.41 (1C), 159.46 (1C). $^{19}\text{F-NMR}$ (235 MHz, CDCl_3 , 300 K) δ (ppm) = -156.22 (m, 1F), -156.17 (m, 1F), -139.23 (m, 1F), -139.18 (m, 1F). IR (ATR): ν = 2919, 2853, 1799, 1780, 1731, 1644, 1504, 1485, 1405, 1384, 1314, 1211, 1182, 1091, 1050, 1005, 852, 758, 714, 611. ESI-MS (m/z): $[\text{M}^+]$ calculated for $\text{C}_{23}\text{H}_{30}\text{F}_4\text{O}_6$, 478.4; found, 501.4 ($[\text{M} + \text{Na}^+]$). EA (%) calculated: C 57.70, H 6.30, F 15.88, O 20.06. Found: C 58.17, H 6.34, F 15.86.

Synthesis of 3-(dodecyloxy)-2,3,5,6-tetrafluoromethanol (5).

To a solution of 4-(dodecyloxy)-2,3,5,6-tetrafluorobenzoic acid (3c) (15.0 g, 39.6 mmol, 1.0 eq.) in dry THF (100 mL), BH_3 -THF solution (1 M) (139 mL, 139.0 mmol, 3.5 eq.) was slowly added with a dropping funnel at -15°C . Then, the reaction mixture was allowed to warm to room temperature and stirred for 1 hour, followed by 2 hours at 50°C . To complete the reaction, the mixture was cooled to 0°C and diluted HCl was added, and the mixture was stirred for 1 hour. The organic phase was separated, and the aqueous phase was extracted three times with diethyl ether. The combined organic phases were pre-dried with brine and dried over Na_2SO_4 . The solvent was evaporated and the crude product purified by column chromatography (eluent: hexane-EtOAc = 95/5) to obtain the product as a viscous liquid in 13.1 g (91%) yield. $^1\text{H-NMR}$ (300 MHz, CDCl_3 , 300 K) δ (ppm) = 0.88 (t, 3J = 7.00 Hz, 3H), 1.26 (m, 16H), 1.45 (m, 2H), 1.76 (p, 3J = 6.7 Hz, 2H), 4.21 (t, 3J = 6.7 Hz, 2H), 4.78 (t, 3J = 4.8 Hz, 2H). $^{13}\text{C-NMR}$ (75 MHz, CDCl_3 , 295 K) δ (ppm) = 14.15 (1C), 22.71 (1C), 25.52 (1C), 29.25 (1C), 29.37 (1C), 29.53 (1C), 29.58 (1C), 29.65 (2C), 29.86 (1C), 31.93 (1C), 55.76 (1C), 75.34 (1C), 111.92 (1C), 137.79 (1C), 139.59 (1C), 142.81 (1C), 143.93 (1C), 147.15 (1C). $^{19}\text{F-NMR}$ (235 MHz, CDCl_3 , 300 K) δ (ppm) = -146.49 (m, 1F), -146.55 (m, 1F), -157.21 (m, 1F), -157.58 (m, 1F). EA (%) calculated: C 62.62, H 7.74, F 20.85, O 8.78. Found: C 62.73, H 7.70, F 20.70.

Synthesis of 2-[2-[2-(2-methoxyethoxy)ethoxy]ethoxy]ethyl *p*-tosylate. An aqueous solution of NaOH (w = 0.5, 1.5 mL) was slowly added to tetra(ethylene glycol) monomethyl ether (4.2 g, 20.0 mmol, 1.0 eq.) with vigorous stirring at 0°C . After stirring for 30 min, a solution of *p*-toluenesulfonyl chloride (TsCl) (4.6 g, 24.0 mmol, 1.2 eq.) dissolved in THF (20 mL) was slowly added to the reaction mixture and the solution was stirred at 0°C for another 3 h. Then the solution was poured into water and extracted with CHCl_3 . The combined organic solution was washed with water and brine. After drying with MgSO_4 , the solvent was removed *in vacuo*. The crude product was purified by column chromatography (eluent: ethyl acetate) to obtain 2-[2-[2-(2-methoxyethoxy)ethoxy]ethoxy]ethyl *p*-tosylate in 4.9 g (68%) yield as a colorless oily liquid. $^1\text{H-NMR}$ (CDCl_3 , 300 MHz) δ (ppm) = 2.43 (s, 3H), 3.36 (s, 3H), 3.60 (m, 14H), 4.14 (t, 3J = 4.9 Hz, 2H), 7.33 (d, 3J = 7.5 Hz, 2H), 7.78 (d, 3J = 7.5 Hz, 2H). $^{13}\text{C-NMR}$ (75 MHz, CDCl_3 , 300 K) δ (ppm) = 21.75 (1C), 59.13 (1C), 68.74 (1C), 69.35 (1C), 70.60 (2C), 70.67 (2C), 70.81 (1C), 71.99 (1C), 128.07 (2C), 129.91 (2C), 133.01 (1C), 144.89 (1C).

Synthesis of 2-[2-[2-(2-Methoxyethoxy)ethoxy]ethoxy]ethyl-4-(dodecyloxy)-2,3,5,6-tetrafluorophenyl (6). A solution of compound 5 (4.4 g, 12.2 mmol, 1.0 eq.) and Cs_2CO_3 (12.0 g, 26.7 mmol, 3.0 eq.) in dry THF (70 mL) was stirred at RT for 1 h before the addition of 2-[2-[2-(2-methoxyethoxy)ethoxy]ethoxy]ethyl *p*-tosylate (4.7 g, 12.8 mmol, 1.1 eq.). After 16 h stirring at 75°C , the reaction mixture was cooled to room temperature, and the white precipitate was filtered off. The precipitate was washed several times with THF and EtOAc. The organic extracts were combined, washed with brine and dried over Na_2SO_4 . The solvent was evaporated and the crude product purified by column chromatography (eluent: hexane-ethyl acetate = 55/45) to give compound 6 in 4.3 g (65%) yield as a pale yellow liquid. $^1\text{H-NMR}$ (300 MHz, CDCl_3 , 300 K) δ (ppm) = 0.86 (t, 3J = 6.5 Hz, 3H), 1.24 (m, 16H), 1.43 (m, 2H), 1.74 (p, 3J = 6.7 Hz, 2H), 3.36 (s, 3H), 3.54 (m, 2H), 3.64 (m, 14H), 4.19 (t, 3J = 6.8 Hz, 2H), 4.61 (t, 4J = 1.7 Hz, 2H). $^{13}\text{C-NMR}$ (75 MHz, CDCl_3 , 295 K) δ (ppm) = 14.19 (1C), 22.78 (1C), 25.62 (1C), 29.33 (1C), 29.44 (1C), 29.61 (1C), 29.65 (1C), 29.73 (2C), 29.97 (1C), 32.01 (1C), 59.09 (1C), 60.17 (1C), 70.07 (1C), 70.54 (1C), 70.61 (1C), 70.69 (2C), 70.71 (1C), 70.77 (1C), 72.04 (1C), 75.43 (1C), 109.43 (1C), 138.06 (1C), 139.62–139.88 (1C), 142.35–142.56 (1C), 144.57 (1C), 147.30 (1C). $^{19}\text{F-NMR}$ (235 MHz, CDCl_3 , 300 K) δ (ppm) = -144.91 (1F), -144.96 (1F), -157.50 (1F), -157.55 (1F). IR (ATR): ν = 2923, 2854, 1653, 1493, 1468, 1386, 1353, 1294, 1248, 1199, 1130, 1103, 1048, 998, 935, 881, 852, 761, 722, 633. ESI-MS (m/z): $[\text{M}^+]$ calculated for $\text{C}_{28}\text{H}_{46}\text{F}_4\text{O}_6$, 554.7; found, 577.7 ($[\text{M} + \text{Na}^+]$). EA (%) calculated: C 60.60, H 8.40. Found: C 60.24, H 8.56.

Synthesis of 4-decyloxybenzoic acid (7). 4-Hydroxybenzoic acid (5.5 g, 40.0 mmol, 1.0 eq.) was dissolved in ethanol solution (100 mL) of KOH (6.7 g, 120 mmol, 3.0 eq.). To this solution 1-bromodecane (10.0 g, 40.0 mmol, 1.0 eq.) was added drop by drop with a syringe under constant stirring. The reaction mixture was refluxed over 16 h. Then conc. HCl was added to hydrolyze the obtained potassium salt ($\text{pH} = 2$). A white precipitate was obtained. The precipitate was dissolved in hot toluene. The insoluble fraction was filtered off and the solvent was evaporated under reduced pressure from the remaining product solution yielding the crude product as a white solid. The crude product was recrystallized to give compound 7 in 8.5 g (69%) yield as a white crystalline solid.

$^1\text{H-NMR}$ (300 MHz, CDCl_3 , 300 K) δ (ppm) = 0.87 (t, 3J = 6.73 Hz, 3H), 1.26 (s, 12H), 1.45 (p, 3J = 6.82 Hz), 1.79 (p, 3J = 6.60 Hz), 4.00 (t, 3J = 6.55 Hz, 2H), 6.94 (d, 3J = 8.89 Hz, 2H), 8.07 (d, 3J = 8.85, 2H), 9.56 (s, 1H). $^{13}\text{C-NMR}$ (63 MHz, CDCl_3 , 300 K) δ (ppm) = 13.86 (1C), 25.69 (1C), 28.80 (1C), 29.04 (2C), 29.08 (1C), 29.27 (2C), 31.62 (1C), 68.10 (1C), 113.89 (2C), 121.05 (1C), 132.04 (2C), 163.38 (1C), 171.58 (1C). EA (%) calculated: C 73.35, H 9.41. Found: C 73.16, H 9.46.

Synthesis of (2-Oxo-1,3-dioxolan-4-yl)methyl 4-decyloxybenzoate (8). To a solution of 1-ethyl-3-(3-dimethylaminopropyl) carbodiimide hydrochloride (EDC) (30.0 mmol, 6.0 eq.) and 4-dimethylaminopyridine (DMAP) (5.5 mmol, 1.1 eq.) in dry DCM (120 mL) 4-decyloxybenzoic acid (7) (5.0 mmol, 1.0 eq.) was added under cooling with ice/water and stirred for one hour. Then, glycerol 1,2-carbonate (30.0 mmol, 6.0 eq.) was

added, and the mixture was stirred for 2 days at room temperature. The reaction mixture was then poured into a saturated NH_4Cl aqueous solution, the organic phase was separated and the aqueous phase was extracted with CH_3Cl . The organic phase was pre-dried with brine and dried over Na_2SO_4 . The solvent was evaporated *in vacuo* and the crude product purified by column chromatography (eluent: $\text{DCM-MeOH} = 95/5$) to obtain the product as a white solid in 0.8 g (42%) yield. $^1\text{H-NMR}$ (300 MHz, CDCl_3 , 300 K) δ (ppm) = 0.87 (t, $^3J = 6.95$ Hz, 3H), 1.26 (m, 12H), 1.45 (p, $^3J = 7.46$ Hz, 2H), 1.79 (p, $^3J = 6.62$ Hz, 2H), 4.00 (t, $^3J = 6.57$ Hz, 2H), 4.20 (dd, $^2J = 8.74$ Hz, $^3J = 5.62$ Hz, 1H), 4.49 (dd, $^2J = 12.60$ Hz, $^3J = 3.83$ Hz, 1H), 4.53 (dd, $^2J = 12.60$ Hz, $^3J = 3.10$ Hz, 1H), 4.63 (t, $^3J = 8.59$ Hz, 1H), 5.04 (m, 1H), 6.91 (d, $^3J = 8.93$, 2H), 7.95 (d, $^3J = 8.91$, 2H). $^{13}\text{C-NMR}$ (75 MHz, CDCl_3 , 295 K) δ (ppm) = 14.25 (1C), 22.79 (1C), 26.06 (1C), 29.16 (1C), 29.42 (1C), 29.46 (1C), 29.66 (2C), 32.00 (1C), 63.45 (1C), 66.25 (1C), 68.41 (1C), 74.16 (1C), 114.44 (2C), 120.80 (1C), 131.99 (2C), 154.69 (1C), 163.69 (1C), 165.82 (1C). IR (ATR): $\nu = 2953, 2918, 2851, 1781, 1714, 1605, 1511, 1399, 1282, 1254, 1162, 1047, 780$. EA (%) calculated: C 66.65, H 8.00. Found: C 65.84, H 7.98.

Acknowledgements

Funding from Consortium für elektrochemische Industrie der Wacker Chemie AG is gratefully acknowledged. We thank Prof. Gasteiger for the opportunity to measure conductivity at his chair.

Notes and references

- R. L. Kerr, S. A. Miller, R. K. Shoemaker, B. J. Elliott and D. L. Gin, *J. Am. Chem. Soc.*, 2009, **131**, 15972.
- T. Ichikawa, M. Yoshio, A. Hamasaki, J. Kagimoto, H. Ohno and T. Kato, *J. Am. Chem. Soc.*, 2011, **133**, 2163.
- K. Hoshino, K. Kanie, T. Ohtake, T. Mukai, M. Yoshizawa, S. Ujiie, H. Ohno and T. Kato, *Macromol. Chem. Phys.*, 2002, **203**, 1547.
- B. Scrosati, *Electrochim. Acta*, 2000, **45**, 2461.
- M. Armand and J.-M. Tarascon, *Nature*, 2008, **451**, 652.
- J. B. Goodenough and Y. Kim, *Chem. Mater.*, 2010, **22**, 587.
- K. Xu, *Chem. Rev.*, 2004, **104**, 4303.
- M. Wakihara, *Mater. Sci. Eng.*, 2001, 109.
- J.-P. Gabano, in *Lithium Batteries*, Academic Press, New York, 1983, p. 17.
- Z. Zhu, A.-G. Einset, C.-Y. Yang, W.-X. Chen and G. E. Wnek, *Macromolecules*, 1994, **27**, 4076.
- T. Kato, *Science*, 2002, **295**, 2414.
- T. Kato, *Angew. Chem., Int. Ed.*, 2010, **49**, 7847.
- T. Kato, N. Mizoshita and K. Kishimoto, *Angew. Chem.*, 2006, **118**, 44.
- V. Percec and G. Ungar, *Adv. Mater. Opt. Electron.*, 1994, **4**, 303.
- T. Ohtake, M. Ogasawara, K. Ito-Akita, N. Nishina, S. Ujiie, H. Ohno and T. Kato, *Chem. Mater.*, 2000, **12**, 782.
- Y. Zheng, J. Lui, G. Ungar and P. V. Wright, *Chem. Rec.*, 2004, 176.
- K. Kishimoto, M. Yoshio, T. Mukai, M. Yoshizawa, H. Ohno and T. Kato, *J. Am. Chem. Soc.*, 2003, **125**, 3196.
- Y. Akachi, K. Kawamura and N. Koide, *Polym. Adv. Technol.*, 2001, **12**, 422.
- T. Kato, *Chem. Mater.*, 2000, **12**, 782.
- K. Kishimoto, T. Suzawa, T. Yokota, T. Mukai and T. Kato, *J. Am. Chem. Soc.*, 2005, **127**, 15618.
- K. Hoshina, K. Kanie, T. Ohtake, T. Mukai, M. Yoshizawa, S. Ujiie, H. Ohno and T. Kato, *Macromol. Chem. Phys.*, 2002, **203**, 1547.
- H. Shimura, M. Yoshio, A. Hamasaki, T. Mukai, H. Ohno and T. Kato, *Adv. Mater.*, 2009, **21**, 1591.
- T. Ohtake, K. Ito, N. Nishina, H. Kihara, H. Ohno and T. Kato, *Polym. J.*, 1999, **11-2**, 1155.
- N. A. A. Rossi and R. West, *Polym. Int.*, 2009, **58**, 267.
- I. Ichikawa, M. Yoshio, A. Hamasaki, T. Mukai, H. Ohno and T. Kato, *J. Am. Chem. Soc.*, 2007, **129**, 10662.
- D. W. Bruce, P. Metrangolo, F. Meyer, T. Pilati, C. Präsang, G. Rednati, G. Terraneo, S. G. Wainwright and A. C. Whitwood, *Chem.-Eur. J.*, 2010, **16**, 9511.
- G. Sandford, *Tetrahedron*, 2003, **59**, 437.
- Z. Luo, Q. Zhang, Y. Oderaotoshi and D. P. Curran, *Science*, 2001, **291**, 1766.
- Y. Sasada, H. Monobe, Y. Ueda and Y. Shimizu, *Mol. Cryst. Liq. Cryst.*, 2009, **509**, 186.
- M. P. Krafft and J. G. Riess, *Chem. Rev.*, 2009, **109**, 1714.
- X. Cheng, M. Kumar Das, S. Diele and C. Tschierske, *Langmuir*, 2002, **18**, 6521.
- R. Nandi, H. K. Singh, S. K. Singh, B. Singh and R. K. Singh, *Spectrochim. Acta, Part A*, 2014, **128**, 248.
- <http://www.dow.com/ethyleneglycol/about/properties.htm>, accessed Nov 12, 2014.
- Y. Chernyak, *J. Chem. Eng. Data*, 2006, **51**, 416.
- L. M. Blinov, in *Structure and Properties of Liquid Crystals*, Springer, 2011.
- I. Dierking, in *Texture of Liquid Crystals*, Wiley-VCH, Weinheim, 2003.
- M. Yoshio, T. Mukai, H. Ohno and T. Kato, *J. Am. Chem. Soc.*, 2004, **126**, 994.
- M. Lee and B.-K. Cho, *Chem. Mater.*, 1998, **10**, 1894.
- <http://www.als-japan.com>, accessed June 6, 2014.
- K. Ito-Akita, N. Nishina, Y. Asai, H. Ohno, T. Ohtake, Y. Takamitsu and T. Kato, *Polym. Adv. Technol.*, 2000, **11**, 529.
- S. Liang, U. H. Choi, W. Liu, J. Runt and R. H. Colby, *Chem. Mater.*, 2012, **24**, 2316.
- M. Duclot, F. Alloin, O. Brylev, J. Y. Sanchez and J. L. Souquet, *Solid State Ionics*, 2000, **136-137**, 1153.
- D. Fragiadakis, S. Dou, R. H. Colby and J. Runt, *J. Chem. Phys.*, 2009, **130**, 064907.
- C. T. Imrie, M. D. Ingram and G. S. McHattie, *J. Phys. Chem. B*, 1999, **103**, 4132.
- H. Kataoka, Y. Saito, Y. Uetani, S. Murata and K. Kii, *J. Phys. Chem. B*, 2002, **106**, 12084.
- G. E. Murch, *Solid State Ionics*, 1982, **7**, 177.
- I. M. Ward, N. Boden, J. Cruickshank and S. A. Leng, *Electrochim. Acta*, 1995, **40**, 2071.

- 48 I. Nicotera, C. Oliviero, W. A. Henderson, G. B. Appetecchi and S. Passerini, *J. Phys. Chem. B*, 2005, **109**, 22814.
- 49 M. Kunze, Y. Karatas, H.-D. Wiemhöfer, H. Eckert and M. Schönhoff, *Phys. Chem. Chem. Phys.*, 2010, **12**, 6844.
- 50 Y. Saito, K. Hirai, S. Murata, Y. Kishii, K. Kii, M. Yoshio and T. Kato, *J. Phys. Chem. B*, 2005, **109**, 11563.
- 51 J. E. Tanner, *J. Chem. Phys.*, 1970, **52**, 2523.
- 52 P. Stilbs, *Prog. Nucl. Magn. Reson. Spectrosc.*, 1987, **19**, 1.
- 53 J. Kösters, M. Schönhoff and A. N. Stolwijk, *J. Phys. Chem. B*, 2013, **117**, 2527.
- 54 M. Joost, M. Kunze, S. Jeong, M. Schönhoff, M. Winter and S. Passerini, *Electrochim. Acta*, 2012, **86**, 330.